Fluorescence sensing techniques for vegetation assessment

Lawrence A. Corp, Elizabeth M. Middleton, James E. McMurtrey, Petya K. Entcheva Campbell, and L. Maryn Butcher

Active fluorescence (F) sensing systems have long been suggested as a means to identify species composition and determine physiological status of plants. Passive F systems for large-scale remote assessment of vegetation will undoubtedly rely on solar-induced F (SIF), and this information could potentially be obtained from the Fraunhofer line depth (FLD) principle. However, understanding the relationships between the information and knowledge gained from active and passive systems remains to be addressed. Here we present an approach in which actively induced F spectral data are used to simulate and project the magnitude of SIF that can be expected from near-ground observations within selected solar Fraunhofer line regions. Comparisons among vegetative species and nitrogen (N) supply treatments were made with three F approaches: the passive FLD principle applied to telluric oxygen (O_2) bands from field-acquired canopy reflectance spectra, simulated SIF from actively induced laboratory emission spectra of leaves at a series of solar Fraunhofer lines ranging from 422 to 758 nm, and examination of two dual-F excitation algorithms developed from laboratory data. From these analyses we infer that SIF from whole-plant canopies can be simulated by use of laboratory data from active systems on individual leaves and that SIF has application for the large-scale assessment of vegetation. © 2006 Optical Society of America

OCIS codes: 120.0280, 120.6200, 120.5700, 170.6280.

1. Introduction

A major goal of the U.S. Carbon Cycle Science program is to monitor carbon dioxide (CO_2) uptake by vegetation. Biological carbon (C) sequestration is driven by nitrogen (N) availability, as N is involved in photochemical processes and is one of the primary resources that regulate plant growth. Large-scale monitoring of these processes is currently possible only with remote-sensing systems that rely heavily on passive reflectance (R) information. Fluorescence (F) emitted from chlorophyll (Chl), or ChlF, is directly related to photochemical reactions and has been extensively used for the elucidation of the photosynthetic pathways. Recent studies have shown that ChlF can be extracted from high-resolution reflectance spectra of vegetation[1–3]; this has been made possible by advances in passive F instrumentation, which facilitate remote acquisition of solar-induced fluorescence (SIF). The goal of this effort is to evaluate the potential of emerging F methodologies for determining vegetation parameters related to photosynthetic function and carbon sequestration dynamics in plants.

Chl is the major plant pigment associated with harvesting solar energy for conversion to photochemical energy and use in CO_2 assimilation for the production of sugars and other organic compounds. Under optimal growth conditions, most light absorbed by plant Chls and carotenes is utilized in photosynthesis; less than 3% is dissipated as heat or as F. The magnitude of F emissions (EMs) varies with exposure of plants to light and other environmental conditions and is governed by Chl concentration. The highest F yield occurs when competing photochemical processes do not drain energy available for photosynthesis and heat dissipation is low. As certain nutrients play primary roles in photosynthesis and

L. A. Corp (lcorp@hydrolab.arsusda.gov) and L. M. Butcher are with Science Systems and Applications, Inc., Lanham, Maryland 20706. E. M. Middleton is with the Biospheric Sciences Branch, NASA/Goddard Space Flight Center, Greenbelt, Maryland 20771. J. E. McMurtrey is with the Hydrology & Remote Sensing Laboratory, Agricultural Research Service, U.S. Department of Agriculture, Beltsville, Maryland 20705. P. K. Entcheva Campbell is with the Joint Center for Earth Systems Technology, University of Maryland, Baltimore County, Baltimore, Maryland 21250.

Received 3 May 2005; revised 19 August 2005; accepted 25 August 2005.

0003-6935/06/051023-11$15.00/0

© 2006 Optical Society of America

Chl synthesis, their deficiencies can be detected on the basis of changes in F, especially that of N.[4–8]

ChlF is manifested as red fluorescence (RF) and far-red fluorescence (FRF).[9] RF has been attributed primarily to Chls associated with photosystem II, whereas FRF has been attributed to antenna Chls of both photosystems II and I.[10–12] The RF/FRF ratio could relate to changes in the distribution of excitation (EX) energy between the two photosystems and has been extensively studied as an indicator of Chl content and stress condition in plants.[9,13–15] In addition to ChlF, F from vegetation occurs throughout the ultraviolet (UV-A) to visible regions, with EM maxima occurring in the UV-A, blue (BF), and green (GF).[16,17] Several investigations have demonstrated relationships to plant health and growth condition for these F regions and their ratios.[5,16,18–22]

The remote sensing of F over land has proved challenging because the relatively weak EMs from vegetation must be differentiated from the more-intense R signals. One solution is to utilize the Fraunhofer line depth (FLD) principle with high spectral resolution R spectra. The FLD principle uses the dark lines in the spectrum of light reaching the Earth's surface reported by Joseph Fraunhofer in 1817 and subsequently identified as either solar or telluric (i.e., atmospheric) in origin. This approach employs the dark regions to potentially differentiate F from the solar irradiance continuum with sufficient resolution for low-Earth-orbit observations by interferometer-type passive satellite systems. This technology has been suggested as a passive method for detecting vegetation stress from orbit.[23,24] In particular, the FLD method has been suggested as a means for extracting ChlF from R spectra in the telluric oxygen (O_2) bands centered at 688 and 760 nm. However, only a few instruments capable of remotely detecting solar-induced ChlF have successfully demonstrated variations in the F signal that can be ascribed to vegetation stress.[25–29]

The focus of this investigation is on the F signal from terrestrial vegetation as viewed from near-ground levels. The current study was designed to (1) develop generalized three-dimensional EX by an EM spectral matrix (EEM) for foliage represented by two herbaceous and three woody plant species from actively induced F studies; (2) present an approach to simulating SIF from the EEM and discrete EX spectral data at the foliar level; (3) determine from field spectra the magnitude of SIF that can be obtained at ground level from terrestrial vegetation assemblages within the telluric O_2 absorption bands; and (4) compare the relative ability of three F approaches to discriminate experimental vegetation treatments by use of the passive FLD applied to the telluric O_2 bands, the simulated SIF at solar Fraunhofer lines, and two active dual-EX algorithms.

2. Materials and Methods

A. Plant Material

Plant material was collected from several field sites at the U.S. Department of Agriculture's Beltsville Agricultural Research Center, Beltsville, Maryland. Deciduous trees were sampled from a multiyear experiment in which six-year-old saplings of tulip poplar (*Liriodendron tulipifera* L.), red maple (*Acer rubrum* L.), and sweet gum (*Liquidambar styraciflua* L.) were planted in the ground in 2001. N was applied in the form of urea, and concentrations were varied from 0.004 to 0.001 M to simulate augmented levels of atmospheric N deposition. Measurements acquired during September and October 2004 were utilized for this study, and the data are presented as a composite of all treatments sampled.

The cornfield site is part of an intensive test site for a multidisciplinary project entitled Optimizing Production Inputs for Economic and Environmental Enhancement (OPE) to develop new farming strategies that conserve natural resources while maintaining or increasing long-term farm profitability. Corn (*Zea mays* L.) N-treatment plots large enough to capture the spatial variability of crop and soil parameters were established within the OPE field site. The experimental design was a randomized complete block with treatment groups of 280, 140, 70, and 0 kg N/ha, which provided a range of plant growth and condition. The rate of 140 kg N/ha was recommended by the University of Maryland Soil Test Laboratory for optimum corn production on the OPE sandy loam soil. Measurements were acquired in August 2004 at the grain fill (R3) reproductive stage. Average daily photosynthetically active radiation and temperature up to this period were 220 W/m^2 and 22 °C with 393 mm of total rainfall.

The soybean [*Glycine max* (L.) Merr.], Illini cultivar, along with two Chl *b* deficient isolines (BV4 & T135) related to the Illini parent were grown in two forms of growth medium: soil with the agrobacterium rhizobium and the full compliment of nutrients required for optimal growth, and a sterile perlite growth medium in which no rhizobium species were allowed to infect the roots. Nutrient solutions were applied weekly to plants in perlite to provide all nutrients required for optimal plant growth. The experiment was divided into two planting–measurement periods, each allowing for 45 days of growth. Average daily photosynthetically active radiation and temperature for the two planting periods were 181 W/m^2 and 20 °C for the first planting period (May–June 2003) and 175 W/m^2 and 23 °C for the second period (July–September 2003).

B. Active Fluorescence Measurements

A spectrofluorometer (Fluorolog-II, Spex Industries, Edison, New Jersey) was used to collect EEMs and discrete EX spectra on excised leaf samples from the plant canopies. This spectrofluorometer utilizes two 0.22 m double spectrometers with gratings of 1200 grooves/mm. A 450 W xenon lamp was attached to the EX spectrometer with entrance and exit slits set to 2 mm, yielding a 3.2 nm bandpass for EX radiation from 250 to 700 nm. Fluctuations in lamp intensity were corrected by use of a beam split-

ter to deliver a portion of the EX radiation to a silicon photodiode. This response was used to generate correction factors for equalizing changes in lamp intensity as a function of wavelength. The EM spectrometer was attached to a photon-counting photomultiplier tube, which was radiometrically calibrated to yield linear measures of intensity throughout the EM wavelength range of 400–800 nm. The entrance and exit slits for both the EX and EM spectrometers were set to 2 mm, permitting a 3.2 nm bandpass. The data acquisition interval was set to 5 nm, and leaf samples were held in place by a nonfluorescent anodized aluminum solid sample holder.

The relative magnitudes and number of EM bands received from vegetation vary with EX wavelength. The EX by EM matrix (EEM) is a three-dimensional F matrix with the horizontal coordinates corresponding to EX and EM wavelengths while the vertical coordinate corresponds to the EM intensities. Leaf EMs were determined over the wavelength range of 400–800 nm, and EX characteristics were determined over the wavelength range of 300–700 nm. In addition to EEMs, several discrete EX spectra were collected at 5 nm data acquisition intervals starting at 300 nm and ending 20 nm short of several select Fraunhofer features.

C. Simulated Solar-Induced Fluorescence from Actively Induced Excitation Spectra

Xenon arc lamps are frequently used in laboratory situations to simulate solar energy in the visible spectrum. However, the spectral profile of the arc lamp does not precisely match the solar spectrum. Therefore a calibrated spectral radiometer was inserted in the sample compartment of the Fluorolog II spectrofluorometer and the radiometric intensity was measured as a function of illumination wavelength [Fig. 1(a)]. These data were then compared with the solar spectrum of a clear day that yielded a photosynthetic photon flux density of 1660 μmol m^{-2} s^{-1} or 400 W m^{-2} nm^{-1}. Correction factors were then developed and applied such that the postcorrection spectral profile and intensity of the xenon illumination source closely resembled that of the solar spectrum [Fig. 1(b)]. Simulated SIF intensities (mW m^{-2} nm^{-1}) were then obtained through integration of monochromatically acquired EX spectra from 300 nm to the wavelength that was 20 nm short of the Fraunhofer line being simulated, to prevent cross contamination of the EX source and the EM response. We used a revised edition of Rowland's table of solar spectrum wavelengths to select major solar Fraunhofer lines based on proximity to F features and line strength.[30] The projected F intensity in each line was calculated based on a Fraunhofer equivalent width (a measure of line strength for a perfectly black line of sharp edges absorbing the same amount of energy as the real line). The simulated SIF approach was used to provide estimates of F intensity per nanometer, whereas multiplication with line equivalent widths provided estimates for the final F intensity

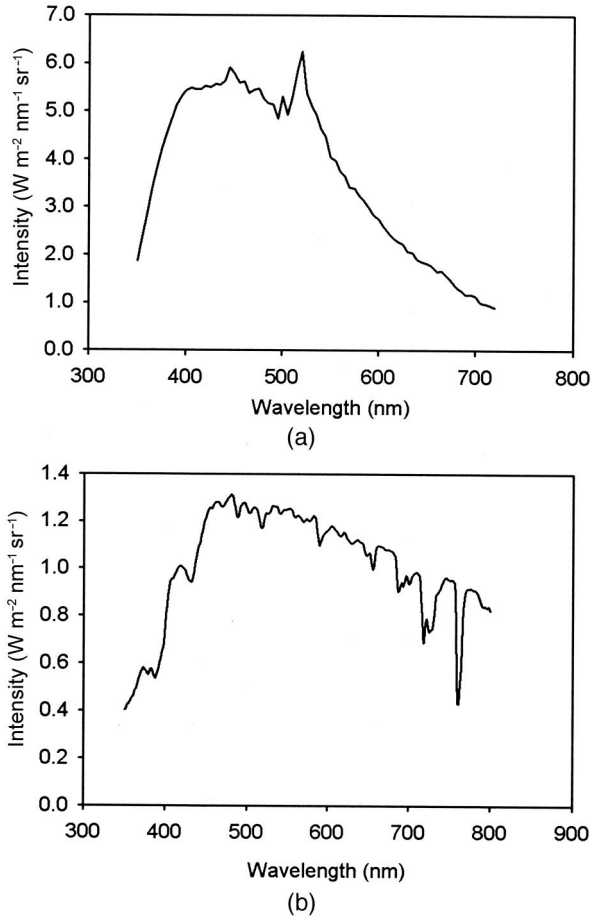

Fig. 1. Spectral profiles: (a) xenon arc lamp, (b) solar spectrum at a total irradiance level of 400 W/m^2.

(mW m^{-2} sr^{-1}) expected within selected Fraunhofer lines at the ground level.

D. Fraunhofer Line Depth Determination of Solar-Induced Fluorescence in the Atmospheric O_2 Bands

The FLD principle was applied to discriminate the relatively weak *in situ* vegetation F in-fill of the telluric O_2 bands that fall within the ChlF region. The major telluric O_2 features located at 688 and 760 nm and with a FWHM of 4 and 7 nm, respectively, are formed from the merging of a series of narrowband molecular oxygen absorptions by the Earth's atmosphere. We used the following algebraic expressions of the FLD principle adapted from Plascyk[31] to obtain canopy R and F from vegetated surfaces:

$$R = (c - d)/(a - b), \tag{1}$$

$$F = d - Rb = (ad - cb)/(a - b), \tag{2}$$

where a and b represent the reference panel radiance in and out of each O_2 feature and c and d represent the target radiance of a and b, respectively. F within a Fraunhofer feature can also be expressed as the relative stationary yield (f = F/a), a dimensionless number representing the degree to which radiance

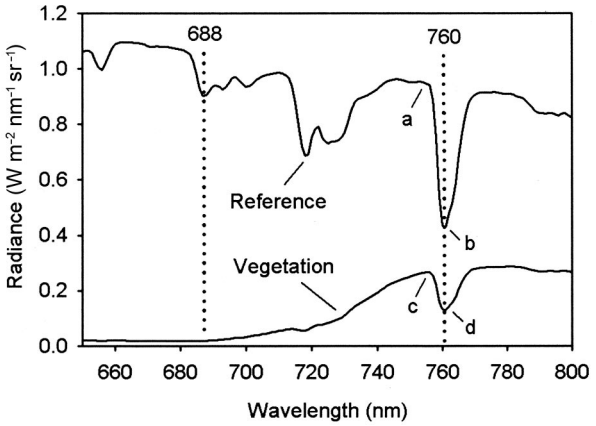

Fig. 2. Radiance measured in the red through far-red spectral region. Telluric O_2 bands are denoted with dotted lines, and a, b, c, and d correspond to points in Eqs. (1) and (2) for the FLD determination of far-red SIF.

within a relatively dark Fraunhofer line is augmented.

We used a spectroradiometer (ASD-FR FieldSpec Pro, Analytical Spectral Devices, Inc., Boulder, Colorado) to measure canopy radiance 1 m above plant canopies with a 22° field of view and a 0° nadir view zenith angle. A second, cross-calibrated, ASD radiometer was used in a similar viewing geometry over a Spectralon reference panel (Labsphere, North Sutton, New Hampshire) to track changes in solar irradiance simultaneously. The ASD spectroradiometers use a 512 channel silicon photodiode array overlaid with an order separation filter to provide 3 nm FWHM spectral resolution at a 1.4 nm sampling resolution, which is sufficient for the quantification of F and R within the major telluric O_2 features (Fig. 2). Measurements were obtained on a clear day in a 2 h window near solar noon and yielded an average photosynthetic photon flux density of 1660 μmol m^{-2} s^{-1}.

E. Biophysical Measurements

Biophysical analysis of plant canopies occurred *in situ* where possible; otherwise the uppermost fully expanded leaves or third leaf from the terminal were excised from the plant canopy, immediately placed in water-filled sample holders, and transported to the laboratory for further analysis. The leaf-area index (LAI) of the corn canopy was measured with the LAI 2000 plant canopy analyzer (LI-COR Inc., Lincoln, Nebraska). Five sets of LAI measurements (a single one above the canopy and four below the canopy) were acquired at predetermined sample locations throughout each treatment plot. Corn grain yields were based on hand-harvested samples obtained from five plants per plot at locations where foliar F, Chl concentrations, and N determinations were obtained. Grain samples were oven dried at 50 °C before weighing. Photosynthetic capacity (A_{max}; μmol CO_2 m^{-2} s^{-1}) was determined *in situ* with a LI-COR 6400 photosynthetic system (LI-COR, Inc.) fitted with a leaf fluorometer chamber. A_{max} was determined under controlled conditions of 2000 μmol m^{-2} s^{-1} of photosynthetically active radiation, saturating CO_2 concentration (1000 parts in 10^6), controlled leaf temperature (22 °C), and relative humidity (~35%). A_{max} and light-adapted steady-state ChlF (Fs) were obtained simultaneously in the field before excision of leaves for laboratory measurements. The LI-COR 6400 F parameter is detected by a broadband sensor centered at 700 nm and provides a measure of total photons fluoresced per second from both ChlF bands. Leaf Chl *a* and Chl *b* and total carotene concentrations were determined from freshly cut leaf disks (2.54 cm^2) that were placed in 3.5 ml of dimethyl sulfoxide and sealed for 36 h at 25 °C. Absorption spectra were obtained with a dual-beam spectrophotometer (Lambda 40, Perkin-Elmer, Norwalk, Connecticut), and pigment concentrations were determined by procedures outlined by Wellburn.[32] The remainder of each leaf sample was oven dried at 50 °C and ground to pass through a 1 mm mesh. Total leaf C and N determinations were obtained by the Dumas combustion method[33] by the University of Delaware Soil Testing Program, Newark, Delaware.

A mixed model analysis of variance (SAS, Inc., Cary, North Carolina) was used to assess the separability of plant parameters and F features with respect to treatment effects. Least-significant digit (LSD) mean separations were deemed significant at $p \leq 0.05$.

3. Results

A. Analysis of Plant Growth

For various levels of N fertilization in field corn, leaf parameters (A_{max}, Chl, foliar N) and crop parameters (LAI, grain yield) increased with N level (Table 1). LAI was similar for the two N fertilization rates $\geq$ 140 kg N/ha, whereas significant LAI decreases were obtained for treatments $\leq$ 70 kg N/ha, where a difference of $\geq$0.27 LAI was significant by the $LSD_{0.05}$ means comparison procedure. Both the Chl *a*:*b* and C:N ratios exhibited decreases with increasing N supply, with minimum significant differences of 0.178 and 1.68 ($LSD_{0.05}$), respectively. Overall, the analysis of corn growth and condition at lower N availability was consistent with classic symptoms of N deficiency.

The soybean Illini cultivar exhibited significantly higher Chl content and C:N ratios than the Chl *b* isolines (Table 1). As expected, Chl *b* was suppressed in the BV4 and T135 isolines; this was expressed in elevated Chl *a*:*b* ratios. Unexpectedly, foliar N levels were also significantly higher for the Chl *b* deficient isolines, along with *in vivo* UV-A F, indicating potentially higher rubisco (the CO_2 fixing enzyme) and protein content.[17] This result was also evidenced by the higher trend in A_{max} achieved by the Chl *b* isolines.

B. Excitation by Emission Matrix

The generalized EEM for vegetation is shown in Fig. 3 as a surface plot depicting the average EM intensity from foliage represented by two crops (corn and soy-

Table 1. Effects of Treatment on Biophysical Measures of Plant Growth and Condition

Source of Variation		Chl $a + b$[a]	Chl a	Chl b	Chl a:b	C (%)	N (%)	C:N	A_{max}[b]	LAI	Yield[c]
Corn	280[d]	65.5 a[e]	45.4 a	20.2 a	2.29 d	47.9 a	3.67 a	13.1 c	39.8 ab	3.14 a	10062 a
	140	56.5 b	40.6 b	16.1 b	2.56 c	47.9 a	3.34 b	14.4 c	42.4 a	2.98 a	8010 b
	70	50.5 c	37.5 b	13.1 c	2.86 b	47.4 a	2.83 c	16.9 b	38.4 b	2.54 b	6833 b
	0	33.7 d	25.4 c	8.4 d	3.08 a	46.2 b	2.08 d	23.4 a	26.9 c	2.27 c	4614 c
$LSD_{0.05}$ ($n = 60$)[f]		5.46	3.64	2.11	0.178	0.68	0.208	1.68	3.02	0.269	1178
Soybean	Illini	24.7 a	18.7 a	6.04 a	3.07 a	45.6 ab	2.15 b	25.8 a	21.2 a		
	T135	14.4 b	11.7 b	2.77 b	4.42 b	46.4 a	3.45 a	15.4 b	26.1 a		
	BV4	11.9 b	9.7 b	2.18 b	4.65 b	45.0 b	3.65 a	13.4 b	26.4 a		
$LSD_{0.05}$ ($n = 66$)		5.05	3.98	1.11	0.350	1.14	0.527	4.23	ns		
Poplar		42.5 b	31.6 b	11.0 b	2.97 a	49.6 a	1.77 a	28.94 a	24.4 a		
Maple		39.2 b	28.8 b	10.5 b	2.78 b	49.9 a	1.81 a	28.72 a	22.1 a		
Gum		50.8 a	35.9 a	15.0 a	2.40 c	49.6 a	1.73 a	29.82 a	23.0 a		
$LSD_{0.05}$ ($n = 48$)		4.66	3.17	1.58	0.164	ns	ns	ns	ns		

[a]Chlorophyll (Chl) contents are in micrograms per meter squared.
[b]Photosynthetic units (A_{max}) are in micromoles of CO_2 per meter squared per second.
[c]Gain yields are reported in kilograms per hectare.
[d]Nitrogen treatment levels in field corn are expressed in kilograms of nitrogen per hectare.
[e]Within a treatment group, isoline, or species columnwise means with the same letter are not separable (ns) by the $ANOVA_{LSD_{0.05}}$ means comparison procedure.
[f]Groupwise $LSD_{0.05}$ values indicate the smallest separable source of variation for each variable.

bean) and three deciduous tree species (poplar, gum, and maple). Through a three-dimensional analysis (EX by EM by intensity), consistently occurring F spectral features were noted across species at the wavelength coordinates reported in Table 2. All measured species exhibited pronounced BF, GF, RF, and FRF EM features, with the exception of corn, for which the GF was minimal. The BF and GF features exhibit discrete EX maxima that are induced by UV-B through UV-A radiation. Also, maximized EM intensities from these two bands can be achieved from EX radiation at 347 ± 25 nm and 410 ± 10 nm, respectively. In contrast, the RF and FRF peaks are induced over a wider range of UV-A through visible wavelengths, and each exhibits a similar series of EX maxima at or near 430, 470, and 665 nm. Although the RF and FRF EMs are emitted exclusively through Chl a, these EX maxima coincide with either the absorptive properties of Chl a or the nonfluorescing secondary photosynthetic antenna pigments (e.g., Chl b and carotene) that transfer energy to Chl a. Whereas the existence of the BF, GF, RF, and FRF peaks is well established, this study reveals that EX wavelength regions that produce maximal F intensities are relatively narrow (≤10 nm wide), with the exception of the blue EX region (25 nm wide). Although the central wavelengths of EM features are fairly stable (≤11 nm), there were some variations observed in the peak centers and peak widths (Table 2) associated with species that deserve further study.

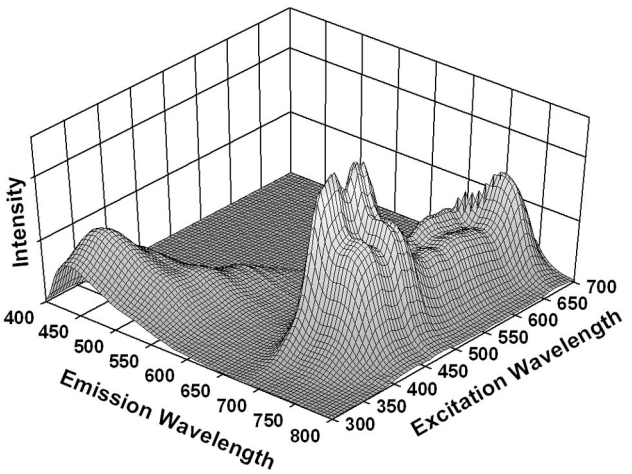

Fig. 3. Generalized vegetation spectral EEM represented by a surface plot, based on the responses from mature, summer foliage for two herbaceous and three woody plant species ($n = 20$).

C. Dual-Wavelength Excitation Ratios

The FRF EX spectra at 740 nm extracted from the vegetation EEM along with absorption spectra of the pure plant pigments (Chl a, Chl b, and carotene) are shown in Fig. 4. An alignment between the ChlF EX maxima and absorption features of the plant pigments is apparent. Inasmuch as ChlF EX spectra are affected by the combined absorption of light by plant pigments, specific F ratios may express the relative changes in these pigment contents. As evidenced here, the *in vivo* Chl a:b ratio showed significant variation with respect to N supply in the corn and in the tree species sampled (Table 1). The soybean parent line Illini and the Chl b deficient isolines BV4 and T135 extended the observed range of Chl a:b ratios from 3.07 to 4.66. Through spectral sensitivity analyses and correlations with spectroscopically determined plant pigment concentrations, specific EX by

Table 2. Mean EX by EM Wavelengths (nm) for EEM Maxima, across Five Plant Species

Fluorescence	Attribute	Species					Vegetation Average
		Corn	Soybean	Poplar	Gum	Maple	
BF	EX	352[a]	346 ± 43	341 ± 5	353 ± 29	342 ± 8	347 ± 25
	EM	443 ± 12	460 ± 6	453 ± 5	446 ± 11	443 ± 14	450 ± 11
GF	EX		400 ± 8	419[a]	409 ± 9	418[a]	410 ± 10
	EM		529 ± 7	538 ± 5	540 ± 11	538[a]	536 ± 8
RF 1	EX	423 ± 12	425 ± 10	437[a]	431 ± 10	436[a]	430 ± 10
	EM	681[a]	688 ± 6	686[a]	691 ± 6	688[a]	687 ± 5
RF 2	EX	482 ± 13	473 ± 7	471 ± 8	467[a]	467[a]	472 ± 8
	EM	681[a]	694 ± 7	690[a]	698 ± 5	693 ± 5	691 ± 7
FRF 1	EX	424 ± 14	424 ± 10	437[a]	432 ± 11	437[a]	430 ± 10
	EM	734[a]	740[a]	740[a]	740[a]	740[a]	739[a]
FRF 2	EX	479 ± 14	471 ± 8	471 ± 8	467[a]	467[a]	470 ± 8
	EM	735[a]	740[a]	740[a]	740[a]	743[a]	740[a]
FRF 3	EX	663 ± 15	662 ± 10	669[a]	669[a]	668[a]	665 ± 8
	EM	736[a]	740[a]	740[a]	740[a]	740[a]	739[a]

[a]The standard deviation is less than the data acquisition interval of 5 nm.

EM wavelength combinations were found sensitive to *in vivo* variation in the Chl *a*:*b* ratios. Of these wavelength combinations, the following two normalized difference (ND) dual-wavelength EX ratios were found to have superior performance:

$$\text{ND RF} = (\text{RF}_{\text{EX435}} - \text{RF}_{\text{EX475}})/(\text{RF}_{\text{EX435}} + \text{RF}_{\text{EX475}}), \tag{3}$$

$$\text{ND FRF} = (\text{FRF}_{\text{EX435}} - \text{FRF}_{\text{EX475}})/(\text{FRF}_{\text{EX435}} + \text{FRF}_{\text{EX475}}). \tag{4}$$

These dual-EX algorithms normalize the differences of the RF or the FRF at two distinct monochromatic EX wavelengths that are important in Chl absorption, namely, 435 and 475 nm. Both algorithms were found sensitive to N supply in the field corn: the ND FRF algorithm provided three levels of separation, whereas the ND RF algorithm distinguished all four N treatment levels (Table 3). Further, linear relationships were observed between the dual-EX algorithms and Chl *a*:*b* ratios (r^2 = 0.81 − 0.83; Fig. 5). For the corn and soybean crop species the normalization of these ratios enabled a single linear fit to be applied across the monocot and dicot crop species. However, the ND RF and ND FRF algorithms were not so effective in tracking the less dynamic Chl *a*:*b* variations associated with the tree species.

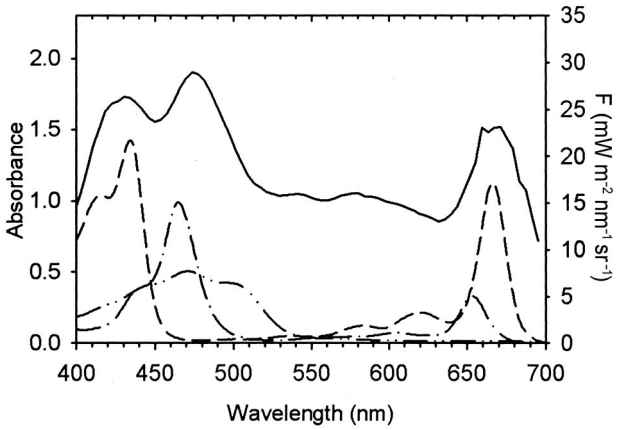

Fig. 4. ChlF intensity from intact leaves (solid curve), extracted from the EEM shown in Fig. 3, varies as a function of EX wavelength. This EX spectrum originates from the primary plant pigment Chl *a* (dashed curve) but is also affected by light absorptions from the secondary pigments Chl *b* (dashed–dotted) and carotene (dashed–dotted–dotted).

D. Active Simulated Solar-Induced Fluorescence

The SIF observed in each is induced by wavelengths in the UV–visible solar spectrum leading to each specific line. Correction of the distribution of EX energy from the xenon arc lamp reduced the contribution from UV stimulated ChlF and accentuated the effect of ChlF by wavelengths greater than 500 nm. We generated the level of SIF expected from vegetation as a function of EM wavelength (Fig. 6) by applying the SIF approach to EX spectra. The locations of select solar Fraunhofer features across the SIF EM spectrum are shown by dashed curves. A summary of the strongest solar Fraunhofer features surrounding peak EM areas in the wavelength range from 422.7 to 758.6 nm is given in Table 4. F intensities (mW m^{-2} nm^{-1} sr^{-1}) calculated from the integration of solar-corrected EX spectra are listed in column 4, in which rows set in italic type identify the major Fraunhofer features that fell closest to the actively induced peak EM areas as identified in Table 2. Several major Fraunhofer features were identified in the blue–green region of the spectrum from 422 to 542 nm and had equivalent widths that ranged from 0.0478 to 0.368 nm. Estimates of the within-line F, adjusted for linewidth, are given in column 5 of Table 4. The within-line blue–green simulated SIF intensities yielded relatively low signal levels [0.0018 to

Table 3. Comparison of Steady-State ChlF Techniques for Vegetation Assessment

Source of Variation		F_s[b]	Dual F EX Ratios		Active Simulated SIF[a]			Passive FLD SIF[a]		
			NDRF	NDFRF	RF	FRF	NDR:FR	RF	FRF	NDR:FR
Corn	280[c]	524.0 a	−0.109 a[d]	−0.201 a	4.56 a	8.15 a	−0.293 a	21.7 a	16.9 a	0.125 a
	140	522.6 a	−0.087 b	−0.165 b	3.43 b	6.36 b	−0.302 a	25.0 b	15.9 a	0.222 b
	70	516.2 a	−0.059 c	−0.149 b	3.53 b	6.76 ab	−0.336 b	25.0 b	9.5 b	0.450 c
	0	492.8 b	−0.027 d	−0.101 c	3.38 b	6.29 b	−0.307 ab	36.3 c	7.0 c	0.675 d
$LSD_{0.05}$ (n = 60)[e]		11.10	0.021	0.018	0.99	1.43	0.033	2.73	1.44	0.063
Soybean	Illini	290.5 a	0.064 a	−0.041a	4.65 a	8.80 a	−0.318 a			
	T135	264.4 a	0.324 b	0.153 b	3.54 b	5.21 b	−0.217 b			
	BV4	260.9 a	0.374 b	0.212 b	3.87 ab	5.49 b	−0.149 b			
$LSD_{0.05}$ (n = 66)		ns	0.063	0.061	0.84	1.03	0.084			
Poplar		566.6 a	0.061 a	−0.074 a	1.48 a	5.03 a	−0.548 a	35.5 a	9.1 a	0.589 a
Maple		592.8 a	0.053 a	−0.111 b	1.51 a	5.18 a	−0.560 a	34.5 a	9.1 a	0.568 a
Gum		580.2 a	0.082 a	−0.079 ab	1.24 a	4.40 a	−0.566 a			
$LSD_{0.05}$ (n = 48)		ns	ns	0.033	ns	ns	ns	ns	ns	ns

[a]F intensities are reported in milliwatts per square meter divided by nanometers per steradian.
[b]Fs is expressed as total photons per second from both ChlF peaks (RF + FRF).
[c]Nitrogen treatment levels on field corn are expressed in kilograms of nitrogen per hectare.
[d]Within a treatment group, isoline, or species columnwise means with the same letter are not separable (ns) by the $ANOVA_{LSD_{0.05}}$ means comparison procedure.
[e]Groupwise $LSD_{0.05}$ values indicate the smallest separable source of variation for each variable.

0.0157 mW m^{-2} sr^{-1}] compared with SIF in the ChlF regions [0.0208 to 0.1397 mW m^{-2} sr^{-1}] that can potentially be retrieved from 656 to 758 nm. The Fraunhofer features that provided the highest signal for the detection of blue, green, red, and far-red SIF were H_β at 486 nm, Mg at 518 nm, H_α at 656 nm, and Fe_I at 751 nm, respectively. Note that the wavelengths of these features do not necessarily coincide with the wavelengths of the respective EM maxima.

The simulated SIF intensities based on actively induced foliar F for corn calculated at the RF and FRF EM maxima varied only slightly with N fertilization level (Table 3). For the 2004 crop, the 280 kg N/ha fertilization rate led to significant increases in photosynthetic pigment content (Table 1) and ChlF (Table 3) compared with the remaining treatments. The bulk of the solar-induced RF for corn was induced by radiation from 400 to 500 nm, with much lower contributions stimulated from other regions of the spectrum, whereas the far-red SIF has an added component from EX radiation extending past 650 nm. The UV-induced ChlF accounts for only as much as 4% of the total simulated solar-induced ChlF, indicating that commonly employed active systems that use UV EX sources may not track SIF as well as systems that use a visible EX source.

Similarly for the soybean isoline experiment, the Illini cultivar had the highest photosynthetic pigment content and correspondingly higher simulated SIF intensities (Tables 1 and 3). A significant decrease in ChlF was noted for EX spectra over the Chl b absorption region of 450 to 500 nm for the BV4 and T135 isolines compared with the Illini cultivar. This property appeared in both ChlF bands but was more pro-

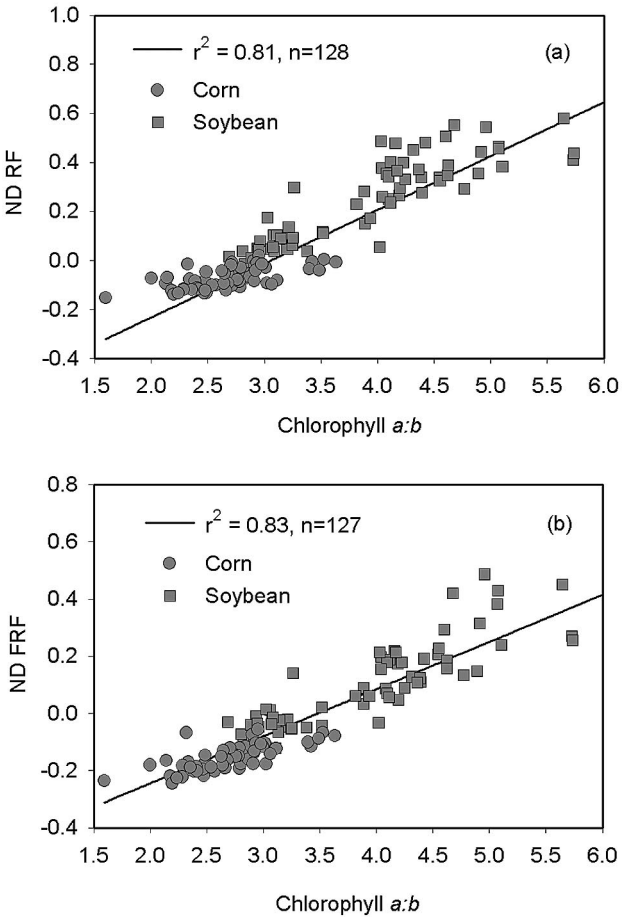

Fig. 5. Selection of discrete wavelengths from EX spectra led to the development of dual EX ratios for the *in vivo* determination of Chl a:b, based on F properties.

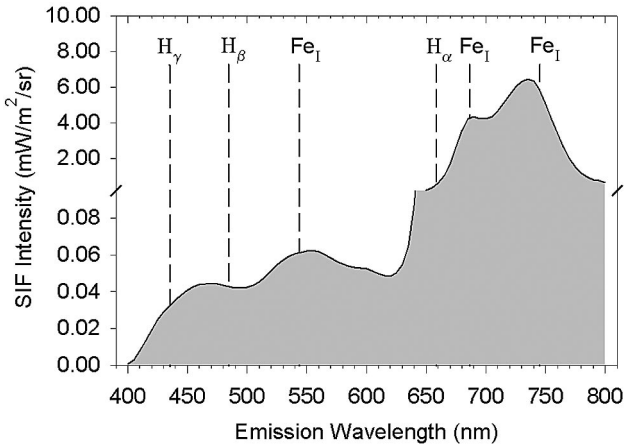

Fig. 6. SIF EM spectrum with dashed lines indicating the position of select Fraunhofer features.

nounced in the FRF band. This observation was further supported by the slightly higher coefficient of determination in Fig. 5 ($r^2 = 0.83$) for FRF compared with RF ($r^2 = 0.81$). The dual F EX and the simulated SIF approaches provided comparable results with respect to separating the F spectral response of the soybean isolines from the Illini parent cultivar (Table 3).

Table 4. Simulated SIF in Fraunhofer Solar Lines as Determined from Leaf EX Spectra[a]

Source[b]	λ (nm)[b]	Equivalent Width (Δλ)[b]	F (mW m^{-2} nm^{-1} sr^{-1})	Within-Line F (mW m^{-2} sr^{-1})
Ca_I	422.67	0.1476	0.0191	0.0028
H_γ	434.05	0.2855	0.0323	0.0092
Fe_I	438.36	0.1008	0.0353	0.0036
H_β	486.13	0.3680	0.0427	0.0157
Mg_I	517.27	0.1259	0.0479	0.0060
Mg_I	518.36	0.1584	0.0512	0.0081
Fe_I	526.96	0.0478	0.0545	0.0026
Fe_I	*532.81*	*0.0375*	*0.0574*	*0.0022*
Fe_I	542.98	0.0285	0.0614	0.0018
H_α	656.28	0.4020	0.3476	0.1397
Fe_I	667.80	0.0122	1.7034	0.0208
Ni_I	676.78	0.0083	2.5996	0.0216
Fe_I	*685.52*	*0.0085*	*4.2257*	*0.0359*
Fe_I	703.82	0.0076	4.3424	0.0330
Ca_I	714.82	0.0157	5.0928	0.0800
Si_I	728.92	0.0116	6.3022	0.0731
Ca_I	732.62	0.0136	6.4565	0.0878
Fe_I	*738.94*	*0.0144*	*6.3357*	*0.0912*
Fe_I	744.58	0.0178	5.8811	0.1047
Fe_I	751.10	0.0221	5.0822	0.1123
Fe_I	758.60	0.0132	3.3715	0.0445

[a]Numbers in italic denote closest proximity to actively induced EM maxima.

[b]The solar atmospheric element or ion (I) source along with the central wavelength location and equivalent width were generated from the second revision of *Rowland's Table of Solar Spectrum Wavelengths*.[30]

E. Fraunhofer Line Depth Determination of Solar-Induced Fluorescence

The FLD principle was applied to the hyperspectral R measurements made over the corn and tree canopies in two telluric O_2 bands that occur in the ChlF region and are centered at 688 and 760 nm. The magnitudes of F retrieved from R ranged from 7 to 36 mW m^{-2} nm^{-1} sr^{-1}. SIF retrieved for RF was greater than for FRF, but the two F bands had opposing trends with respect to N supply (Table 3). The FLD technique applied to data acquired *in situ* provided superior results with respect to sensitivity to corn N supply, compared with the simulated SIF approach in which only the high N treatment group was reliably separable from other groups with RF. In contrast, all four N groups were discriminated for field corn by use of either the passive solar-induced ND RF/FRF ratio or the actively induced ND RF ratio. The two measured tree species had similar values of SIF, with the >3 times higher than FRF. The measured solar-induced ChlF from the tree species ranged from 21 to 36 mW m^{-2} nm^{-1} sr^{-1} for RF and from 7 to 17 mW m^{-2} nm^{-1} sr^{-1} for FRF. These values compare with simulated SIF of 1–5 mW m^{-2} nm^{-1} sr^{-1} for RF and 4–10 mW m^{-2} nm^{-1} sr^{-1} for FRF. These reported F intensities in the O_2 bands are for near-ground observation. Absorption of ChlF by atmospheric O_2 is expected to have a significant attenuation on the signal by the time it reaches orbital altitudes.

4. Discussion

Actively induced F ratios have been shown to relate to the biophysical manifestations of plant stress and, as shown here, F successfully tracked variations in plant parameters (Tables 1 and 3).[9,13–15] In a previous study the far-red/green and the red/blue F ratios (355 nm EX) correlated well with leaf N/C ratios, indicating an application of F to monitor N utilization for C sequestration.[5] The preferred illumination source for most active F field applications is laser light. Although the EEM provides complete spectral profiles for the evaluation of laser wavelengths, active remote F sensing capabilities are still limited by the availability of rugged solid-state pulsed lasers. Advances in laser systems have made the use of multiple–alternating laser excitation sources feasible.[18,21] Further, methods have been presented based on the F excitation ratio to assess nondestructively the types of UV-screening compounds that are present in the leaf epidermis.[21,34]

In our study the ND RF and the ND FRF used two visible excitation wavelengths, 435 and 475 nm, respectively, in normalized dual-wavelength EX ratios for the *in vivo* determination of Chl a/b content. As Chl b enhances the efficiency of light capture for photosynthesis but does not accumulate until sufficient Chl a is synthesized to satisfy photosystem II core complexes, changes in the Chl a/b ratio could potentially be used as a tool for remote monitoring of photosynthetic function.[35] Findings such as these

indicate that active F field instrumentation based on multiple laser EX sources may provide superior sensitivity to alterations in plant growth and condition compared with single EX systems. Although this instrumentation is currently applicable at relatively short distances, the prospects for measuring actively induced F from orbital platforms is feasible but will require further technological developments in diode-pumped solid-state lasers, large-diameter lightweight mirrors, and high-efficiency spectrometers.[36]

Passive SIF emissions from vegetation offer a practical alternative to active space-based F systems.[25,29,37,38] However, for FLD technology to be implemented for the remote assessment of vegetation F, reliable data on steady-state SIF intensities along with results linking SIF to canopy radiation use efficiency are required. Here the complete EEM spectral acquisition facilitated the extraction or interpolation of individual EX spectra, or both, so F in-fill of major Fraunhofer features could be estimated. The Fraunhofer features that yielded the highest observable SIF signal for near-ground observation were H_β at 486 nm (BF) and H_α at 656 nm (RF).

Although the solar-induced BF signal for green vegetation is substantially reduced compared with the ChlF signal, its inclusion in a sensor system would greatly enhance the extent to which the system could monitor the physiological status of vegetation, as evidenced by a number of studies that cite a blue–green/ChlF ratio.[4–7,16,39,40] Further, the solar-induced BF signal from dead–dormant and woody plant materials is roughly two to three times higher than from green plant materials. This in turn would provide a solar-induced BF signal from these materials of $\sim 0.1\ \mathrm{mW\ m^{-2}\ nm^{-1}\ sr^{-1}}$, which equates to $0.037\ \mathrm{mW\ m^{-2}\ sr^{-1}}$ in the H_β Fraunhofer band. Large-scale remote observation of this signal, if used in conjunction with R indices such as the cellulose absorption index[41] and the normalized difference vegetation index, would enhance regional surveys of carbon dynamics, crop residue assessment, and soil conservation practices.

Solar-induced ChlF intensities retrieved from the telluric O_2 absorption features at 688 and 760 nm were of the same orders of magnitude as those obtained in a similar fashion by Liu *et al.*[2] The emitted ChlF increased with Chl content for both EM bands. However, the RF band is subject to reabsorption by Chl, which can lead to decreasing intensities as Chl contents increase. As FRF is outside the absorption features of Chl, it is not subject to reabsorption, and its observed magnitude increases predominantly with Chl content.[14] Owing to the greater bandwidth of the O_2 absorption features, the retrieved near-ground ChlF is several orders of magnitude greater than F retrieved from solar Fraunhofer features. As a result, increased emphasis has been placed on the development of instrumentation explicitly for detecting near-field ChlF in these attenuated regions of the spectrum.[26,29] However, absorption by atmospheric O_2 will increasingly attenuate the F signal relative to sensor altitude. At orbital observation levels, this could negate the advantages of broadband O_2 features and favor the narrowband Fraunhofer line discriminators. Further studies are need with atmospheric absorption estimates to model signal intensities at orbital altitudes and identify properly the advantages and disadvantages of these two passive F techniques.

The primary difference between simulated SIF from actively induced data and SIF determined from passive FLD techniques is that the former is performed on excised plant material in the laboratory (with a summation of a series of monochromatic low-intensity excitations), whereas the latter can be performed *in situ* under polychromatic full Sun. Leaf temperature and photosynthetic photon flux density differentially affect the magnitude of RF and FRF under laboratory-versus-field conditions[2,10,15] and are likely to contribute to the differences in F among the approaches presented here. Nevertheless, the simulated SIF approach provides an opportunity to explore the similarities and differences between actively induced and passive solar-induced vegetation F and project the range of SIF values that one can expect from vegetation under various levels of stress.

5. Conclusions

This research has defined a method for converting monochromatically induced excitation spectra to simulate polychromatic solar-induced fluorescence. Integrated values from actively induced leaf level EX spectra were adjusted, and radiometric estimates of near-ground SIF from vegetation were reported for the primary emission bands. The simulated red SIF intensity at 680 nm ranged from 1 to $5\ \mathrm{mW\ m^{-2}\ nm^{-1}\ sr^{-1}}$, whereas the far red at 740 nm ranged from 4 to $10\ \mathrm{mW\ m^{-2}\ nm^{-1}\ sr^{-1}}$. Of the solar Fraunhofer lines, the H_α line at 656.28 nm and the Fe_I line at 751.1 nm provided the highest signals for near-ground observations of the red fluorescence and far-red fluorescence features. Simulated SIF for the blue–green EM bands were substantially lower for green vegetation but comparable for dead or dormant plant materials, and the H_β line at 486 nm provided the highest blue–green F signal. The simulated SIF data shown here suggest that Fraunhofer line properties have a great effect on the final selection of suitable lines that needs to be balanced with the proximity to the fluorescence EM peaks. Also, simulated SIF from excised plant material showed promise with respect to differentiating plant growth and condition. Increased spatial coverage and repeat temporal measurements should reinforce relationships between solar-induced ChlF and canopy photosynthetic light-use efficiency.

Further sensitivity to plant health parameters can be achieved through active systems and several discrete fluorescence ratios. Maximum EM intensity from blue fluorescence and green fluorescence bands can be achieved from EX at 347 ± 25 and 410

± 10 nm, respectively, whereas the RF and FRF bands exhibited multiple EX maxima: 430 ± 10, 472 ± 8, and 665 ± 8. These RF and FRF EX maxima were strongly associated with the blue and red absorption of Chl *a* and Chl *b* pigments, which led to the development of spectral F excitation ratios for the *in vivo* determination of Chl *a*:*b* content (Fig. 5). Monitoring the variation in these pigment ratios among species and with stress condition could lead to an improved remote-sensing interpretation of species composition and physiological growth condition.

Based on the results from this study, we recommend that specifications for future active F instrumentation require multiple excitation bands. Further studies are needed to establish a compromise between maximized EM intensity versus sensitivity to plant stresses in additional species and stress conditions. The differences in plant physiology and F response found in corn, soybeans, maple, sweet gum, and poplar used in this experiment are estimated to be in the range of what is indicative of other annual and perennial plant species.

References

1. G. Carter, J. Jones, R. Mitchell, and C. Brewer, "Detection of solar-excited chlorophyll *a* fluorescence and leaf photosynthetic capacity using a Fraunhofer line radiometer," Remote Sens. Environ. **55,** 89–92 (1996).
2. L. Liu, Y. Zhang, J. Wang, and C. Zhao, "Detecting solar-induced chlorophyll fluorescence from field radiance spectra based on Fraunhofer line principle," IEEE Trans. Geosci. Remote Sens. **43,** 827–832 (2005).
3. P. Zarco-Tejada, J. Pushnik, S. Dobrowski, and S. Ustin, "Steady-state chlorophyll *a* fluorescence detection from canopy derivative reflectance and double-peak red-edge effects," Remote Sens. Environ. **84,** 283–294 (2003).
4. E. Chappelle, F. Wood, J. McMurtrey, and W. Newcomb, "Laser-induced fluorescence of green plants. 1. A technique for the remote detection of plant stress and species differentiation," Appl. Opt. **23,** 134–138 (1984).
5. L. Corp, J. McMurtrey, E. Middleton, C. Mulchi, E. Chappelle, and C. Daughtry, "Fluorescence sensing systems: *in vivo* detection of biophysical variations in field corn due to nitrogen supply," Remote Sens. Environ. **86,** 470–479 (2003).
6. F. Heisel, M. Sowinska, J. Miehe, M. Lang, and H. Lichtenthaler, "Detection of nutrient deficiencies of maize by laser induced fluorescence imaging," J. Plant Physiol. **148,** 622–631 (1996).
7. G. Langsdorf, C. Buschmann, M. Sowinska, F. Babani, M. Mokry, F. Timmermann, and H. Lichtenthaler, "Multicolour fluorescence imaging of sugar beet leaves with different nitrogen status by flash lamp UV-excitation," Photosynthetica **38,** 539–551 (2000).
8. J. McMurtrey, E. Chappelle, M. Kim, J. Mesinger, and L. Corp, "Development of algorithms for detecting N fertilization levels in field corn (*Zea mays* L.) with laser induced fluorescence," Remote Sens. Environ. **47,** 36–44 (1994).
9. H. Lichtenthaler and U. Rinderle, "Role of chlorophyll fluorescence in the detection of stress conditions of plants," CRC Crit. Rev. Anal. Chem. **19,** 29–85 (1988).
10. G. Agati, Z. Cerovic, and I. Moya, "The effect of temperature on chlorophyll fluorescence: the role of PSI in 735 nm fluorescence," Photochem. Photobiol. **72,** 75–84 (2000).
11. S. Bose, "Chlorophyll fluorescence in green plants and energy transfer pathways in photosynthesis," Photochem. Photobiol. **36,** 725–731 (1982).
12. E. Pfundel, "Estimating the contribution of photosystem I to total leaf chlorophyll fluorescence," Photosynth. Res. **56,** 185–195 (1998).
13. Z. Cerovic, G. Samson, F. Morales, N. Tremblay, and I. Moya, "Ultraviolet-induced fluorescence for plant monitoring: present state and prospects," Agron. Agr. Environ. **19,** 543–578 (1999).
14. A. Gitelson, C. Buschmann, and H. Lichtenthaler, "Leaf chlorophyll fluorescence corrected for re-absorption by means of absorption and reflectance measurements," J. Plant Physiol. **152,** 283–296 (1998).
15. R. Valentini, G. Cecchi, P. Mazzinghi, G. Scarascia Mugnozza, G. Agati, M. Bazzani, P. De Angelis, F. Fusi, G. Matteucci, and V. Raimondi, "Remote sensing of chlorophyll *a* fluorescence on vegetation canopies. 2. Physiological significance of fluorescence signal in response to environmental stresses," Remote Sens. Environ. **47,** 29–35 (1992).
16. E. Chappelle, J. McMurtrey, F. Wood, and W. Newcomb, "Laser-induced fluorescence of green plants. 2. LIF caused by nutrient deficiencies in corn," Appl. Opt. **23,** 139–142 (1984).
17. L. Corp, J. McMurtrey, E. Chappelle, C. Daughtry, and M. Kim, "UV band fluorescence (*in vivo*) and its applications to the remote assessment of N fertilization level," Remote Sens. Environ. **61,** 110–117 (1997).
18. G. Cecchi, P. Mazzinghi, L. Pantani, R. Valentini, D. Tirelli, and P. De Angelis, "Remote sensing of chlorophyll-*a* fluorescence of vegetation canopies. 1. Near and far field measurement techniques," Remote Sens. Environ. **47,** 18–28 (1994).
19. E. Middleton, E. Chappelle, T. Cannon, P. Adamse, and S. Britz, "Initial assessment of physiological response to UV-B irradiation using fluorescence measurements," J. Plant Physiol. **148,** 68–77 (1996).
20. G. Mohammed, W. Binder, and S. Gillies, "Chlorophyll fluorescence: a review of its practical forestry applications and instrumentation," Scand. J. Res. **10,** 383–410 (1995).
21. A. Ounis, Z. Cerovic, J. Briantais, and I. Moya, "Dual-Ex FLIDAR for the estimation of epidermal UV absorption in leaves and canopies," Remote Sens. Environ. **76,** 33–48 (2001).
22. A. Rosema, J. Snel, H. Zahn, W. Buurmeijer, and L. Van Hove, "The relation between laser-induced chlorophyll fluorescence and photosynthesis," Remote Sens. Environ. **65,** 143–154 (1998).
23. J. McMurtrey, E. Middleton, L. Corp, P. Campbell, L. Butcher, E. Chappelle, and W. Cook, "Fluorescence responses from nitrogen plant stress in 4 Fraunhofer band regions," in *2002 IEEE International Geoscience and Remote Sensing Symposium* (Institute of Electrical and Electronics, 2002), pp. 1538–1540.
24. A. Theisen, "Detecting chlorophyll fluorescence from orbit: the Fraunhofer line depth model," in *From Laboratory Spectroscopy to Remote Sensor Spectra of Terrestrial Ecosystems*, R. S. Muttiah, ed. (Springer, 2002), pp. 203–232.
25. G. Carter, A. Theisen, and R. Mitchell, "Chlorophyll fluorescence measured using the Fraunhofer line-depth principle and relationship to photosynthetic rate in the field," Plant Cell Environ. **13,** 79–83 (1990).
26. A. Freedman, J. Cavender-Bares, P. Kebabian, R. Bhaskar, H. Scott, and F. Bazzaz, "Remote sensing of solar-excited plant fluorescence as a measure of photosynthetic rate," Photosynthetica **40,** 127–132 (2002).
27. P. Kebabian, A. Theisen, S. Kallelis, and A. Freedman, "A passive two-band sensor of sunlight-excited plant fluorescence," Rev. Sci. Instrum. **70,** 4386–4393 (1975).
28. J. McFarlane, R. Watson, and A. Theisen, "Plant stress detection by remote measurement of fluorescence," Appl. Opt. **19,** 3287–3289 (1980).

29. I. Moya, L. Camenen, S. Fvain, Y. Goulas, Z. Cerovic, G. Latouche, J. Flexas, and A. Ounis, "A new instrument for passive remote sensing. 1. Measurements of sunlight-induced chlorophyll fluorescence," Remote Sens. Environ. **91,** 186–197 (2004).
30. C. Moore, M. Minnaert, and J. Houtgast, *The Solar Spectrum 2935 Δ to 8770 Δ: Second Revision of Rowland's Preliminary Table of Solar Spectrum Wavelengths*, Natl. Bur. Stand. (U.S.) Monogr. 61 (1966).
31. J. Plascyk, "The MKII Fraunhofer line discriminator (FLD-II) for airborne and orbital remote sensing of solar-stimulated luminescence," Opt. Eng. **14,** 339–346 (1975).
32. A. Wellburn, "The spectral determination of chlorophylls *a* and *b*, as well as total carotenoids using various solvents with spectrophotometers of different resolution," J. Plant Physiol. **144,** 307–313 (1994).
33. G. Bellomonte, A. Constantini, and S. Giammarioli, "Comparison of modified automatic Dumas method and the traditional Kjeldal method for N determination," J. Assoc. Off. Anal. Chem. **70,** 227–229 (1987).
34. Z. Cerovic, A. Ounis, A. Cartelat, G. Latouche, Y. Goulas, S. Meyer, and I. Moya, "The use of chlorophyll fluorescence excitation spectra for the non-destructive *in situ* assessment of UV-absorbine compounds in leaves," Plant Cell Environ. **25,** 1663–1676 (2002).
35. L. Eggink, H. Park, and J. Hoober, "The role of chlorophyll *b* in photosynthesis: hypothesis," Biomed. Cent. Plant Biol. **1,** 2–8 (2001).
36. P. Mazzinghi, G. Cecchi, R. Guzzi, V. Bratina, A. Zuccaro, and L. Gambicorti, "Feasibility of active remote sensing of vegetation fluorescence from space," presented at the 2nd International Workshop on Remote Sensing of Vegetation Fluorescence, Montreal, Canada, 17–19 November 2004.
37. K. Smorenburg, G. Courrèges-Lacoste, M. Berger, C. Buschmann, A. Court, U. Del Bello, G. Langsdorf, H. Lichtenthaler, C. Sioris, M. Stoll, and H. Visser, "Remote sensing of solar induced fluorescence of vegetation," in *Remote Sensing for Agriculture, Ecosystems and Hydrology III*, M. Owe and G. D'Urso, eds., Proc. SPIE **4542,** 178–190 (2001).
38. M. Stoll, T. Laurila, B. Cunin, A. Gitelson, H. Lichtenthaler, and T. Hame, "FLEX—Fluorescence Explorer—a space mission for screening vegetated areas in the Fraunhofer lines," in *Remote Sensing for Earth Science, Oceans, and Sea Ice Applications*, G. Cecchi, E. T. Engman, and E. Zilioli, eds., Proc. SPIE **3868,** 108–119 (1999).
39. C. Bushmann, G. Langsdorf, and H. Lichtenthaler, "Imaging of the blue, green, and red fluorescence emission of plants: an overview," Photosynthetica **38,** 483–491 (2000).
40. M. Kim, J. McMurtrey, C. Mulchi, C. Daughtry, E. Chappelle, and Y. Chen, "Steady-state multispectral fluorescence imaging system for plant leaves," Appl. Opt. **40,** 157–166 (2001).
41. C. Daughtry, E. Hunt, and J. McMurtrey, "Assessing crop residue cover using shortwave infrared reflectance," Remote Sens. Environ. **90,** 126–134 (2004).